NANO LETTERS
Letter
Cite This: Nano Lett. XXXX, XXX, XXX−XXX
pubs.acs.org/NanoLett

Ultrasensitive Monolayer MoS_2 Field-Effect Transistor Based DNA Sensors for Screening of Down Syndrome

Jingxia Liu,[†,∥] Xihua Chen,[‡,∥] Qinqin Wang,[§,∥] Mengmeng Xiao,[†] Donglai Zhong,[†] Wei Sun,[†] Guangyu Zhang,[*,§] and Zhiyong Zhang[*,†]

[†]Key Laboratory for the Physics and Chemistry of Nanodevices and Department of Electronics, Peking University, Beijing 100871, China

[‡]National Research Institute for Family Planning of China, Beijing 100081, China

[§]Beijing National Laboratory for Condensed Matter Physics and Institute of Physics, Chinese Academy of Sciences, Beijing 100190, China

Supporting Information

ABSTRACT: Field-effect transistor (FET) biosensors based on low-dimensional materials present the advantages of low cost, high speed, small size, and excellent compatibility with integrated circuits (ICs). In this work, we fabricated highly sensitive FET-based DNA biosensors based on chemical vapor deposition (CVD)-grown monolayer MoS_2 films in batches and explored their application in noninvasive prenatal testing (NIPT) for trisomy 21 syndrome. Specifically, MoS_2 was functionalized with gold nanoparticles (Au NPs) of an optimized size and at an ideal density, and then, probe DNAs for the specific capture of target DNAs were immobilized on the nanoparticles. The fabricated FET biosensors are able to reliably detect target DNA fragments (chromosome 21 or 13) with a detection limit below 100 aM, a high response up to 240%, and a high specificity, which satisfy the requirement for the screening of Down syndrome. In addition, a real-time test was conducted to show that the biosensor clearly responds to the target DNA at concentrations as low as 1 fM. Our approach shows the potential for detecting the over-expression of chromosome 21 in the peripheral blood of pregnant women and achieving Down syndrome screening.

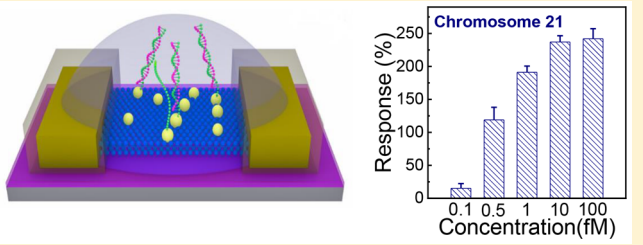

KEYWORDS: *Biosensor, field-effect transistor, DNA, MoS_2, Down syndrome*

A diagnostic device that can recognize multiple disease markers would contribute to various medical applications ranging from point-of-care testing to genomic profiling. The ability to quantitatively differentiate multiple disease markers reveals the identity, concentration, and effect of each heterogeneous effector when assessing a specific disease. Such an ability would further lower the false rate reported with a single-effector test, contributing to an improved diagnostic precision. An example of the application potential of multiplexed quantitative diagnosis is with the early diagnosis of Down syndrome (also known as trisomy 21 syndrome). Down syndrome is caused by the presence of an extra 21st chromosome within the genome and is the most common birth defect (occurring in approximately 1 in 800 births).[1−3] In the absence of a multiplexed quantitative diagnostic device, pregnant women have been examined with ultrasound and indirect biochemical markers (α-fetoprotein, chorionic gonadotropin, and free estriol) with accuracies of 56% and 42%, respectively,[4] which are accompanied by a high misdiagnosis rate, and the diagnostic test (such as amniocentesis) following the wrong screening test results can bring harm/injury to both pregnant women and fetuses. Through polymerization chain reaction (PCR) amplification of the fetal DNA in the pregnant mother's peripheral blood and fluorescence read-out, whole-genome sequencing (WGS)-based noninvasive prenatal testing (NIPT) sequences all the genomic DNA segments in parallel and quantitatively compares the percentage of different chromosomes,[5] which increases the sensitivity for the prenatal detection of Down syndrome.[6] However, owing to the extremely low concentrations of fetal DNA (sub-femtomoles),[7] all of the genomic segments have to be amplified and sequenced via fluorescence read-out. The complex instrumental setups and the resultant high processing cost present challenges to the large-scale application of WGS-based diagnosis at the point of care in the urban and rural areas of developing countries.[2,3] Hence, apart from the expensive WGS method, an urgent need exists to develop a cost-effective NIPT biochip with simple instrumental settings, a fast detection speed, and ultrahigh sensitivity that is programmable to multiple disease markers.

Received: September 20, 2018
Revised: January 20, 2019

DOI: 10.1021/acs.nanolett.8b03818
Nano Lett. XXXX, XXX, XXX−XXX

Owing to their excellent electrostatic properties and high surface-to-volume ratio, nanoscale semiconducting materials, including one-dimensional and two-dimensional materials, have been used to construct label-free biosensors based on platforms such as photoelectric devices, electrochemical devices, and field-effect transistors (FETs).[8−12] Compared with photoelectric or electrochemical devices, FET-based biosensors present the advantages of low cost, high speed, small size, and excellent compatibility with integrated circuits (ICs), leading to the possibility of widespread applications. In the past decade, numerous FET biosensors based on nanomaterials, including silicon nanowires, carbon nanotubes (CNTs), and graphene, have been fabricated.[9,13−18] For Si-nanowire FET biosensors, the minimum diameter of the nanowires, based on current manufacturing technology, is approximately 10 nm,[13,14] which limits the surface-to-volume ratio, and consequently, the sensitivity of the sensor. The weak linkages between CNTs and probe molecules via pyrenebutanoic acid succinimidyl ester (PBASE) or other polymers have resulted in detection with poor repeatability or stability.[19,20] The recent emergence of graphene-based biosensors has attracted extensive interest owing to their extremely thin sensing layer and compatibility with large-scale fabrication. However, owing to the small or even zero band gap of graphene and the small current on-to-off ratio, the resistance change in graphene FET biosensors is very small,[9,18,21] which limits the sensitivity and response of the biosensor. The development of 2D molybdenum disulfide (MoS_2) has brought in a channel material more appropriate than graphene to construct biosensors with a high response and sensitivity because MoS_2 naturally has a large energy band gap.[22,23] However, the recently reported MoS_2 FET biosensors are still in the infancy stage and suffer from poor selectivity, sensitivity, or yield.[24−26] These reported MoS_2 biosensors were built on multilayer materials or covered with a dielectric layer, such as HfO_2, to attach the probe molecules, which further increases the distance between the biomolecular target and the sensing MoS_2 layer and lowers the sensitivity.[24−26] As a result, existing MoS_2 FET-based sensors exhibit a detection limit above 1 pM and a maximum current response under 10%, which is far below the requirement for the screening of Down syndrome.[7]

In this work, we fabricated high-performance FETs based on chemical vapor deposition (CVD)-grown monolayer MoS_2 films and explored their application as multiplexed biosensors for DNA detection. Using a uniform monolayer MoS_2 material and advanced micro- and nanoprocessing methods, the FETs showed excellent electrical performance. Specifically, gold nanoparticles (Au NPs), with an optimized size and of optimum density, were deposited on the MoS_2 channel, and then, the probe DNA was immobilized on the Au NPs to achieve the specific detection of target DNAs, as shown in Figure 1a. Utilizing the high-performance monolayer MoS_2 FET as the sensing platform and the optimized DNA sequence and probe immobilizing scheme to capture target DNA, our sensors present an ultrahigh sensitivity for the reliable detection of DNA with a detection limit of 0.1 fM and a high specificity for 3-nucleotide polymorphism discrimination, meeting the requirements for Down syndrome screening.

First, we fabricated MoS_2 FET arrays on a large scale. MoS_2 films were synthesized on a Si/SiO_2 wafer (300 nm SiO_2) by a CVD approach (for details, see the Methods section). Figure 1b illustrates the fabrication process of the FET-based biosensors. Specifically, MoS_2 FETs were fabricated through

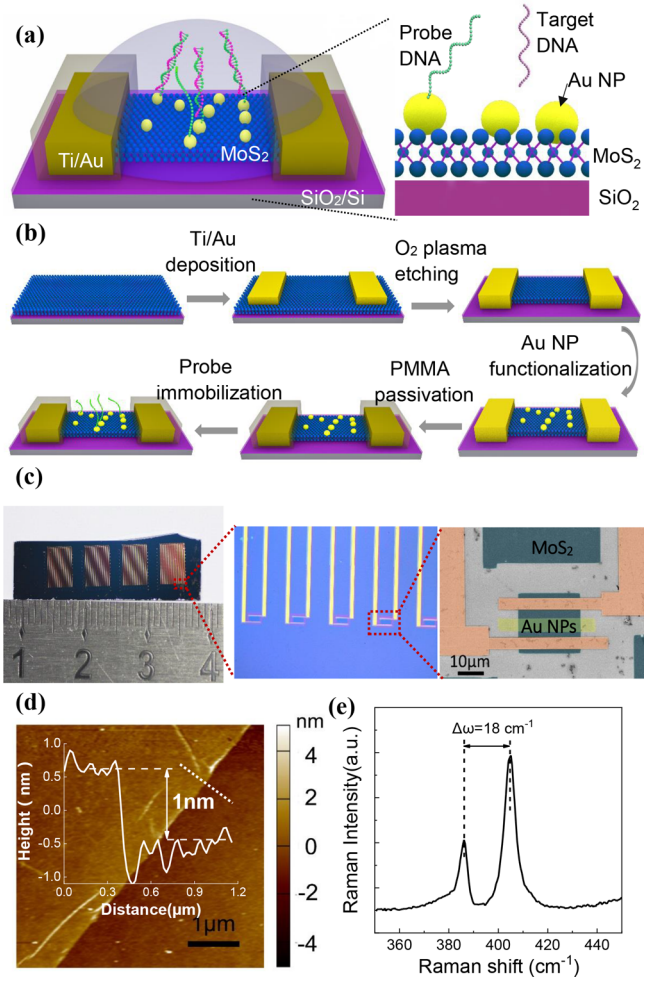

Figure 1. Material characterization and device fabrication of the MoS_2 FET-based biosensor. (a) The structure diagram and (b) fabrication process flow diagram. (c) A typical fabricated chip. The left picture is a photo of a large-area device array, and the middle and right pictures are optical and SEM micrographs of the devices, respectively. The area colored light yellow in the SEM image is the Au NP region in the device channel. (d) The AFM image of MoS_2 indicates that the height of MoS_2 is ca. 0.8 nm. (e) Raman spectroscopy of pristine MoS_2 with peaks at 386.1 and 404.5 cm^{-1}, tested at a 488 nm excitation wavelength.

a standard electron beam lithography (EBL)-based manufacturing process, which has been widely used in our previous works.[27,28] Because of the continuous and homogeneous MoS_2 on the whole substrate (with an area over 3 cm^2), we were able to fabricate FET arrays with large channel sizes on a large scale (Figure 1c), which proved to be of high yield (nearly 100%) and uniformity. The atomic force microscope (AFM) image in Figure 1d shows that the thickness of the MoS_2 layer is less than 1 nm, suggesting the monolayer nature of MoS_2. The Raman spectrum of the MoS_2 layer in Figure 1e shows two peaks (386.1 and 404.5 cm^{-1}) with a spacing of 18 cm^{-1}, further confirming that MoS_2 is a monolayer. The devices were then measured using a silicon substrate as the back gate to assess their uniformity. The transfer curves of five representative MoS_2 FETs with similar dimensions completely coincide (for more details, see Figure S1), indicating the high uniformity of the as-fabricated devices.

DOI: 10.1021/acs.nanolett.8b03818
Nano Lett. XXXX, XXX, XXX−XXX

The second step was forming uniform and dispersed Au NPs on MoS_2 as linkers to immobilize the DNA probe within the device channel. A high density of Au NPs is helpful for increasing the probe density and receiving more captured target molecules on the biosensor. However, a high density of Au NPs will also degrade the conductance and performance of FETs owing to the additional scattering of carriers in the MoS_2 channel. Therefore, FET biosensors require Au NPs in an optimized density and with an ideal size. Initially, instead of the chemical synthesis method (for more details, see Figure S2), physical evaporation, i.e., electron-beam evaporation (EBE) at a low rate of 0.1 Å/s, was chosen in the study to form Au nanoparticles on the MoS_2 channel. Second, the MoS_2 surface promotes the formation of a suitable form of Au NPs owing to the strong interaction between Au and MoS_2.[29−31] The scanning electron microscopy (SEM) image in Figure 2a shows the morphology of the Au NPs formed on SiO_2 and MoS_2 surfaces via the same evaporation process; the sizes of the Au NPs on the surface of MoS_2 are clearly smaller than those on SiO_2, which further demonstrates the interaction between Au and MoS_2. The AFM image presents Au NPs with a thickness of approximately 1 nm (Figure 2b). Therefore, we estimate the Au NPs we processed are approximately 1 nm in size (considering the astigmatism in the SEM image, we estimated this based on AFM results).

As-fabricated MoS_2 FETs with and without Au NP functionalization were also measured in a buffer solution using a phosphate-buffered saline (1× PBS, pH 7.4, containing 0.1 M NaCl) electrolyte as the gate, and the measurement conditions are described in detail in the Methods section. The transfer curves of the fabricated FETs before/after Au NP functionalization were measured in PBS, and the results are shown in Figures 2c and S4. The original MoS_2 FET exhibits high-performance n-type characteristics with an on-state current of up to 10 μA, an on-to-off ratio above 10^6, and a subthreshold swing (SS) of approximately 70 mV/dec All the main device electrical parameters are comparable with or even better than those of the best reported top-gate monolayer MoS_2 FETs.[22,32] Notably, either a small SS or small hysteresis (lower than 30 mV after Au NP functionalization, see the inset in Figures 2f and S6), originating from the ultrahigh efficiency of the electrolyte gate used here,[33,34] is important to the high sensitivity and stability of the biosensor. After functionalization with Au NPs, the FET presents a current that is significantly decreased by nearly an order of magnitude due to the degradation in carrier mobility and p-type doping (positive shift of the threshold voltage) induced by the Au NPs. The p-doping effect of the Au NPs on MoS_2 was further verified by the Raman spectrum measurement, as shown in Figure 2d, which compares pristine MoS_2 (black curve) with Au-functionalized MoS_2 (blue curve). The significantly weakened Raman signal for the Au-functionalized MoS_2 film is likely due to the dense coverage effect of the Au NPs on the MoS_2 surface. Moreover, the blue shift in the A_{1g} peak and the increased spacing between A_{1g} and E^1_{2g} (from 19 to 21 cm^{-1}) reflect that MoS_2 is p-doped by Au NPs.[35,36]

The last step to realize the biosensor was to immobilize the probe DNAs on the Au NPs via Au−S bond formation by immersing the devices in a 100 nM thiolated probe DNA solution in phosphate buffer solution (1× PBS) for 12 h. After probe DNA hybridization, the sensor was then rinsed with PBS to remove unbound probe DNAs. In particular, a buffer solution with a concentration up to 1× PBS was used in the

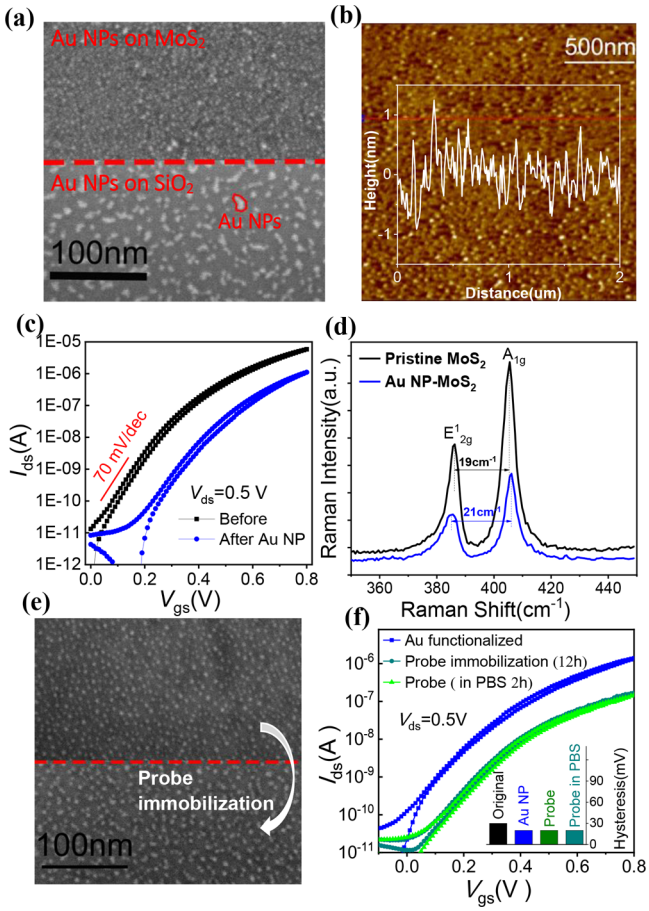

Figure 2. Characteristics of Au NP functionalization and probe DNA immobilization on the MoS_2 FET biosensors. (a) SEM images showing Au NPs (EBE evaporation process for a 0.5 nm Au film at a rate of 0.1 Å/s) on the SiO_2 and MoS_2 surfaces. (b) An AFM image of Au NPs on SiO_2. (c) The transfer curves of the pristine MoS_2 FET (black) and the FET functionalized with Au NPs (blue) were measured in a 1× PBS electrolyte. (d) Raman spectra of pristine MoS_2 (black curve) and Au NP-functionalized MoS_2 (blue curve) under the same test conditions. Each peak height of pristine MoS_2 is approximately 2.5 times that of the Au NP-functionalized MoS_2. (e) SEM images showing Au NPs before and after probe DNA immobilization. The Au NPs were synthesized by evaporating a 0.3 nm Au film. (f) Transfer curves of the Au NP-functionalized MoS_2 FETs before (blue curve) and after (dark green curve) probe immobilization (for 12 h) and further immersion in PBS for 2 h (light green curve). All curves were measured in 0.1× PBS. Inset: hysteresis evolution of the MoS_2 FET at different stages.

hybridization procedure to achieve a small Debye length (0.76 nm here),[12] which promotes hybridization by reducing the range of electrostatic repulsion between probe and target DNA molecules;[13] while in the final test, a more-dilute buffer solution (0.1× PBS) was used to increase the Debye length and sensitivity of the sensor.[18] Figure 2e compares the SEM images of Au NP-decorated MoS_2 sensors before and after DNA hybridization and indicates no visible difference in uniformity and density. In contrast, the mean size of the Au NPs on the probe DNA-functionalized MoS_2 film is slightly larger (approximately 1 nm) than that of the Au NPs on MoS_2 before modification, suggesting that the surface of the Au particles are functionalized with the probe DNAs.

To assess the impact of probe DNA immobilization on the properties of the devices, the transfer curves of the MoS_2 FET

DOI: 10.1021/acs.nanolett.8b03818
Nano Lett. XXXX, XXX, XXX−XXX

before and after probe DNA immobilization were measured in a buffer solution (Figure 2f). The threshold voltage shifts in a positive direction, indicating that probe DNA functionalization introduces p-doping of the MoS_2 channel. We also immersed the device into the PBS solution for 2 h to check the stability of devices after probe DNA functionalization, and there is no visible change in the transfer curves, which reflects that the probe DNA-functionalized MoS_2 FET is stable enough to withstand the next extended test.

Hysteresis is a common defect in the application of nanodevices, including biosensors. Although the back-gated FETs present a large hysteresis (Figure S1), the electrolyte-gated FETs in this work exhibit a hysteresis lower than 50 mV. As shown in the inset of Figure 2f, the hysteresis of electrolyte-gated FETs is approximately 30 mV and further declines to below 20 mV after Au particle modification. Therefore, the statistical experimental data suggest the hysteresis of our FETs after immobilizing the probe are in the range of 0−30 mV, which does not affect the detection results.

Target DNA Detection. The NIPT for Down syndrome requires a highly sensitive sensor to detect the slightly increased concentration of chromosome 21 fragments in maternal blood induced by the fetal cell-free DNA fragments. By comparing the concentrations of the target DNA fragment and the reference fragment, we can monitor whether there is an excessive concentration of chromosome 21, which is the main indicator of Down syndrome. Therefore, similar to the standard WGS-based NIPT, 2 kinds of unique DNA fragments for chromosome 21 (as the target DNA) and chromosome 13 (used here as the reference DNA) should be detected with a high sensitivity by immobilizing their complementary probe DNAs on the FETs. All DNA sequences were designed by the National Research Institute for Family Planning of China with patent protection, and all initial DNA solutions were from this institute. The sequences of the probe DNAs and the target DNAs of chromosomes 21 and 13 are listed in Tables 1 and 2, respectively.

Table 1. Sequences of Chromosome 21 Used in This Work

ssDNA (chromosome 21)	sequence (30mer)
thiolated DNA probe	HS-C6-TGAGTTCCTTCTAGGGAGTCACATTGATGA
complementary DNA target	TCATCAATGTGACTCCCTAGAAGGAACTCA
mismatched DNA	TCATCAATGTGACTGGGTAGAAGGAACTCA

Table 2. Sequences of Chromosome 13 Used in This Work

ssDNA (chromosome 13)	sequence (30mer)
thiolated DNA probe	HS-C6-AGATACCTTACCATCACATGCAAGTGTCTT
complementary DNA target	AAGACACTTGCATGTGATGGTAAGGTATCT

First, the probe DNA, which is complementary to the target DNA (chromosome 21 unique fragments), was used to modify the Au NP-functionalized MoS_2 FET sensors to capture the target. The target DNA measurements with the MoS_2 biosensors were performed in a homemade polydimethylsiloxane (PDMS) microfluidic channel, as shown in Figure S5, into which different solutions were controllably introduced to interact with the device. Before the electrical measurements, the probe DNA-functionalized MoS_2 FET was immersed in a 1× PBS buffer solution containing the target DNA at a certain concentration for 1 h to achieve sufficient hybridization between the probe DNA and target DNA.[14] Then, the FET was electrically measured in 0.1× PBS solution to detect the concentration of the hybridized target DNAs. Notably, every transfer curve was measured 3 times to confirm the stability of the result. Figure 3a shows the transfer curves of the FET

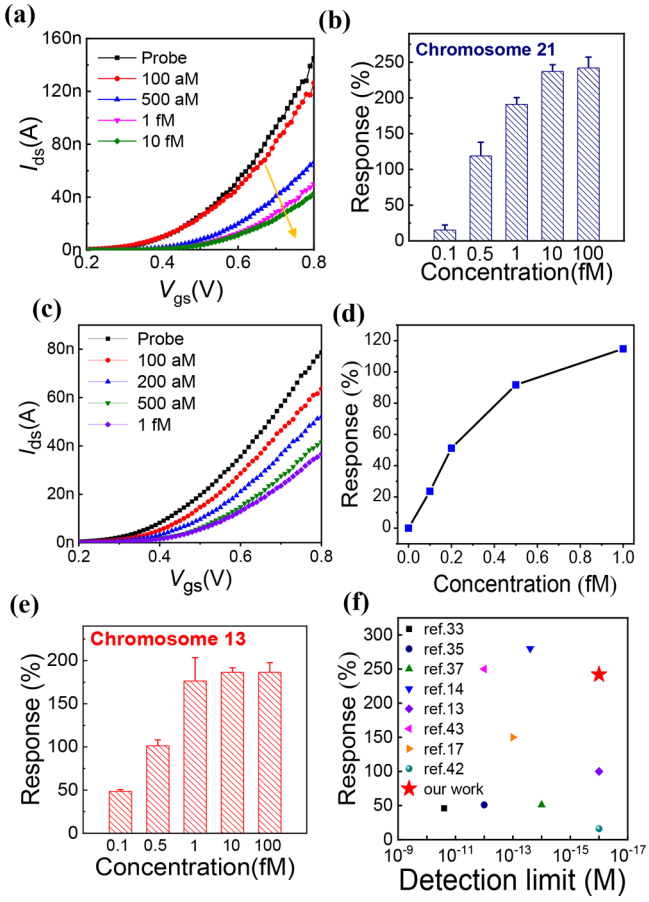

Figure 3. DNA detection measurements of the probe-immobilized biosensors. (a) The response curves for chromosome 21 target DNA solutions with concentrations of 100 aM, 500 aM, 1 fM, and 10 fM. The hybridization time was 1 h for each concentration solution; V_{ds} = 0.5 V. (b) The response-concentration relation retrieved from Figure 3a at V_{gs} = 0.8 V. (c) The linear response-concentration curves for chromosome 21 target DNA for chromosome 21 target DNA solutions with concentrations of 100 aM, 200 aM, 500 aM, and 1 fM; V_{ds} = 0.3 V. (d) The response-concentration relation calculated from Figure 3c at V_{gs} = 0.8 V. (e) The response-concentration relation for chromosome 13 target DNA solutions calculated from Figure S8. (f) The performance comparison between our biosensors and previously reported biosensors based on the detection limit and response. The error bars in panels b and e were extracted from three biosensors on one chip.

biosensor hybridized with the target DNA in different concentrations. The FET biosensor exhibits an evident current drop each time the concentration of target DNAs is increased, indicating that the biosensor is sensitive to chromosome 21 fragments. In particular, the 10 fM target DNA solution induces an almost 70% current drop in the biosensor, as shown in Figure 3a. The response is generally used to benchmark the sensitivity of a biosensor[14,37−40] and is defined as:

DOI: 10.1021/acs.nanolett.8b03818
Nano Lett. XXXX, XXX, XXX−XXX

$$\text{response} = (R - R_0)/R_0 \quad (1)$$

where R and R_0 are the channel resistances of the FET biosensor without and with hybridized target DNA at a fixed gate voltage, respectively. The response of the FET biosensor is calculated by setting V_{gs} to 0.8 V for different measured target DNA concentrations, and the relation between the response and target DNA concentration is shown in Figure 3b. The response increases from 15% (at 100 aM) to 240% (at 10 fM) and then becomes saturated at concentrations above 10 fM. Poor uniformity is one of the most predominant issues hindering the advance of FET biosensors based on nanomaterials. However, in this manuscript, we achieved a high uniformity of FET biosensors in chip through optimizing materials and fabrication processing. We obtained a highly uniform monolayer MoS_2 material and back-gated FETs (as shown in Figure S1), in which the transfer curves of five FETs almost coincide, and the non-uniformity mainly originates from the random diffusion of DNA during probe DNA modification. The devices with large variations (in Figure S6) were fabricated at an early stage. While after further optimization to DNA modification, the biosensors are expected to present a high uniformity in-chip (as shown in Figure 3b).

To study the detection capability of our sensors at sub-femtomole concentrations, we performed in-depth response tests on another biosensor for concentrations linearly ranging from 100 aM to 1 fM. Detailed information about the probe immobilization and measurements is given in Figure S7 and its caption. The transfer curves of the biosensor measured at different target DNA concentrations are shown in Figure 3c and display a clear current drop of approximately 20% at a concentration of 100 aM. The current continuously decreases with increasing concentration and decreases to less than 50% of the original level at a 1 fM concentration. Therefore, the biosensor is sensitive enough to detect sub-femtomole concentrations of the target DNA with an excellent detection limit below 100 aM, which is among the lowest values of reported FET DNA sensors.[13,41] To characterize the linearity of our sensor's response to ultralow concentrations, we plotted a linear curve of the response as a function of concentration from 100 aM to 1 fM, which is shown in Figure 3d. As seen from the curve, the response depends linearly on the concentration below 200 aM, which means that, in principle, we can accurately detect concentrations between 0 and 200 aM as long as the changed current signal can be distinguished from the noise. This work represents the first time that a linear detection of ultralow concentration DNA has been performed. The ultrasensitive DNA sensor, with a detection limit below 100 aM for chromosome 21, provides the possibility of screening for Down syndrome without additional PCR amplification.

We also used the FET-based sensors to detect chromosome 13 fragments as a reference to calibrate the measured concentration of chromosome 21. With the method described before, we performed the probe immobilization process for chromosome 13 and its related concentration detection. The transfer curves of the FET sensor for the DNA of chromosome 13 fragments in different concentrations are shown in Figure S8, and the concentration-dependent response is plotted in Figure 3e. Similar to chromosome 21, the sensors respond well to chromosome 13 in concentrations ranging from 100 aM to 10 fM, with a response at 100 aM larger than that for chromosome 21, proving the good compatibility of our devices for different DNA sequences. The detection limit (or limit of detection, LOD) and response are two key performance metrics for benchmarking a biosensor,[41] and we then compared our MoS_2 FET biosensors with other published FET-based biosensors by using the detection limit and response as the main parameters, as shown in Figure 3f. Compared with the reported high-sensitivity FET-based biosensors using nanomaterials, including Si nanowires[13,14,37,38,40] and CNT biosensors,[17,42,43] our sensors present the best detection limit of 100 aM and are among the sensors with the highest response.

Specificity for specific DNA fragments is essential in NIPT for trisomy 21 syndrome diagnosis. To verify the specificity of our biosensors, we used two probe-immobilized biosensors to detect a customized three-base mismatched DNA sequence of the original for chromosome 21; the sequence is shown in Table 1. The response to 10 fM mismatched DNA is substantially (even 1 order of magnitude) smaller than that to 1 fM complementary target DNA, as shown in Figures 4a and S9, which fully demonstrates the excellent specificity of our biosensors.

We also conducted a real-time test to show how our sensors respond to the target DNA (Figure 4b). In this experiment, the change in current (ΔI_{ds}) under fixed V_{ds} and V_{gs} was monitored as the main parameter. The absolute value of the ΔI_{ds} of a probe DNA-immobilized biosensor clearly increases with the concentration of the introduced target DNA. Within a short hybridization time (400 s), our sensors still clearly distinguished 1 fM target DNA, and the slope of the current decreases continuously with increasing DNA concentration. Lower concentrations are able to be detected with a longer response time in DNA hybridization.[44]

Discussion. Here, we explore the mechanism underlying the current decrease in the sensors after probe DNA immobilization and target DNA hybridization. We quantitatively estimated the number of target DNA molecules (300 DNAs/device) and then the induced carrier density change (3×10^9 /cm^2) in MoS_2 FETs at the 100 aM concentration. While the carrier density in the MoS_2 FETs at $V_{gs} = -0.8$ V is approximately 3×10^{11} /cm^2 (see the details in Part II of the Supporting Information), the charge-transfer-induced channel resistance change is only 1%, indicating the sensing mechanism at a low concentration is not from charge transfer. Because the negative charges in the hybridized DNAs on our biosensors are very close (under 2.3 nm, Debye length[12]) to the MoS_2 channel, the Coulomb potential of these charges in DNA induces scattering to the electrons in the channel. As shown in Figure 4c, revealing the transfer curves of an FET biosensor before and after hybridizing with 100 aM and 100 fM target DNAs, respectively, the change in threshold voltage (V_T) indicates the effect from charge transfer, and the slope change responds to the change in carrier mobility. It is evident that the main mechanism behind the lower current at 100 aM is the charge-induced Coulomb scattering of electrons in the channel. At the higher DNA concentration (100 fM), the current change mechanism simultaneously involves carrier mobility lowering and transferred charges. We confirmed the mechanism of the sensor at high DNA concentration by Raman spectroscopy. It is known that a shift in the A_{1g} peak of the Raman spectrum is related to the doping type and concentration in the 2D MoS_2 layer.[36] We evaporated Au NPs on MoS_2 and immobilized the probe DNA (1 μM) on the Au

DOI: 10.1021/acs.nanolett.8b03818
Nano Lett. XXXX, XXX, XXX−XXX

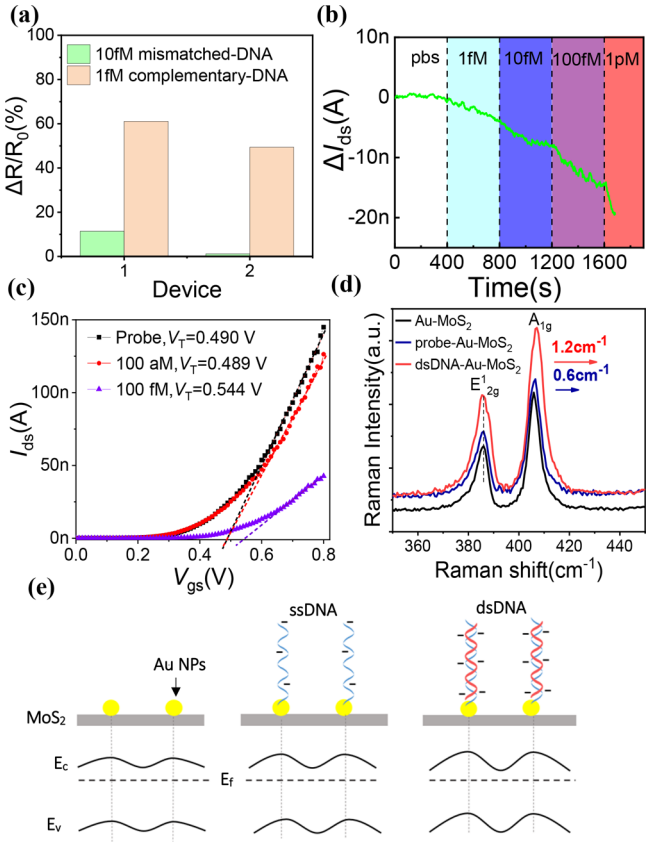

Figure 4. Specificity characteristics of the sensors and the sensing mechanism analysis. (a) The response comparison between mismatched DNA and complementary DNA. The origin response curves of devices 1 and 2 are shown in Figure S9. (b) The timing test of the biosensors. The response time for each concentration is 400 s. (c) The transfer curves changes of the FET biosensors for an ultralow target DNA concentration (100 aM) and a high concentration (100 fM). (d) Raman spectra of the Au NP-MoS_2 hybrid (black curve), the probe-Au NP-MoS_2 hybrid structure (blue curve) and the dsDNA-Au NP-MoS_2 structure (red curve). We processed related structures using high-concentration DNA solutions (1 μM probe DNA and 1 pM target DNA). (e) Schematics of energy band changes for MoS_2 after Au NP deposition, DNA probe immobilization, and target hybridization (for higher concentrations).

NPs. The Raman spectra of the probe-Au-MoS_2 system are compared with the spectra of the Au-MoS_2 hybrid, and a blue shift (0.6 cm^{-1}) of the A_{1g} peak after probe immobilization can be observed in Figure 4d. A similar blue shift induced by DNA hybridization has previously been observed in MoS_2 PL spectra.[45] After hybridization with the complementary DNA target (1 pM), the A_{1g} peak further shifts up in the Raman spectrum, as shown in Figure 4d. Throughout the process, we used DNA solutions whose concentrations were significantly larger than those used in our previous experiments. The two kinds of blueshifts in the A_{1g} peak indicate that both probe DNA immobilization and target DNA hybridization induce p-type doping in the MoS_2 channel, as indicated by previous results.[13,14,38,40] Hence, we conclude that the main mechanism behind the sensor's current drop for DNA at relatively high concentrations is the p-doping of the channel. As shown in Figure 4e, the p-doping effect of the probe DNA or target DNA should lead to a decrease in the number of electrons within local regions of the MoS_2 channel[8,15] and then cause a reduction in the current.

Compared with previously reported MoS_2 FET biosensors,[24−26] we achieved an ultrahigh detection limit (100 aM), high response (240%), and excellent selectivity, which potentially satisfy the essential requirement for Down syndrome screening. The high sensitivity and big response of the FET biosensor mainly originate from two factors. The first is the use of high-quality and uniform monolayer MoS_2 as the channel because the ultrathin semiconducting channel is extremely sensitive to surface dopants. Second, the Au NPs, of suitable size and in the appropriate density, functionalized on the MoS_2 channel serve as excellent linkers for the probe DNA and contribute greatly to the high performance of the FET-based sensors. In addition, while the FET sensor was mainly demonstrated in the detection of chromosome 21 for Down syndrome, it can also be used as a universal sensor platform to detect most types of receptors, including proteins, viruses, antibodies, and nucleotides simply by replacing the probe molecules.

In conclusion, we fabricated high-performance FET biosensors based on CVD-grown monolayer MoS_2 films in batches and demonstrated their application to NIPT for trisomy 21 syndrome. Specifically, Au NPs, with optimized size and in the appropriate density, were functionalized on the MoS_2 channel, and then, probe DNAs were immobilized to achieve the specific detection of target DNAs. The fabricated FET biosensors are capable of reliably detecting target DNA fragments (chromosomes 21 or 13) with a detection limit below 100 aM, a high response up to 240% and a high specificity, showing their potential for detecting chromosome 21 over-expression in the peripheral blood of pregnant women and achieving Down syndrome screening. Our work provides a good reference for high-sensitivity DNA detection with other 2D-material FET sensors and opens the door to direct gene profiling and disease diagnostics with rapidity, high sensitivity, and low cost.

Methods. *Preparation of the Monolayer MoS_2 Film.* The monolayer MoS_2 film was grown on an SiO_2 (300 nm)/p++Si substrate via a three-temperature zone CVD growth process. Sulfur (S) (99.9%) and molybdenum trioxide (MoO_3) (Alfa Aesar 99.999%) were used as precursors and loaded in zones 1 and 2, respectively. The typical distance between the two sources was 22 cm. The SiO_2/Si substrates were placed in zone 3. The temperatures of the zones of S, MoO_3, and the substrate were 119, 540, and 760 °C, respectively. MoS_2 was then synthesized at 760 °C for 20 min. During growth, argon was used as the carrier gas at a flow rate of 130 sccm, and the pressure in the chamber was maintained at 1 Torr. Details of the CVD growth of the monolayer MoS_2 have been reported in our previous work.[46]

The height of MoS_2 was characterized by an AFM (MultiMode IIId, Veeco Instruments, Inc.) by patterning and etching a window in the monolayer MoS_2 thin film. Room-temperature Raman spectra were recorded via 488 nm laser excitation with a confocal spectrometer using a 50× long-working-distance objective and grating with 1800 grooves per millimeter. The morphology of the Au NPs was characterized by SEM (FEI Company, XL30 SFEG).

Fabrication and Measurement of MoS_2 FET-Based Biosensors. To fabricate the MoS_2 FET array, EBL and subsequent O_2-plasma etching were carried out to pattern the MoS_2 channel region. Then, the source and drain contacts were patterned via EBL, deposition of a Ti/Au film (5 nm/40 nm) and a standard lift-off process. We applied a Ti/Au film

DOI: 10.1021/acs.nanolett.8b03818
Nano Lett. XXXX, XXX, XXX−XXX

with a thickness of 5 nm/70 nm to serve as leads and pads, which were achieved using a similar process. To test in the electrolyte, we designed the lead length to be 5 mm to keep the pads away from the solution. Subsequently, we opened windows in the middle of the channel via EBL and evaporated Au NPs in the windows at a rate of 0.1 Å/s by EBE. Finally, the wafer was coated with PMMA 50k, and the regions at the channels and pads were exposed through EBL for contact with the solution or electrical testing probes. The electrical performance of the FETs was measured by using a Keithley 4200 system and a probe station (Summit 11000, Cascade Microtech.)

Initial DNA initial solutions at a concentration of 100 μM were from the National Research Institute for Family Planning of China. Other concentrations of DNA solution were obtained from serial dilution from high to low concentrations according to a 10:1 ratio, and the buffer diluent was PBS.

The home-built PDMS microfluidic channel system shown in Figure S5 allowed different sample solutions to flow into the channel and interact with the sensors of the chip in approximately 60 μL volumes. The inlet and outlet of the microfluidic channel were connected to tubes for analytic injection and removal, and a Ag electrode, inserted through one of the tubes to reach the microfluidic channel, served as the reference electrode. The pad regions of the chip were specifically kept away from the PDMS channel for direct testing on the probe station. The hybridization of target DNAs across all experiments was allowed to proceed for 1 h at room temperature, with the reference electrode and source and drain terminals grounded.

Real-Time Test of Target DNA. Specifically, 0.1× PBS buffer was added to sensors functionalized with probe DNA to establish a baseline current. After a stable reading was obtained, different concentrations of target DNA were sequentially introduced to obtain the current change relative to the baseline current. We set the DNA hybridization time for each concentration to 400 s and changed to a higher concentration after every 400 s.

■ ASSOCIATED CONTENT

Supporting Information

The Supporting Information is available free of charge on the ACS Publications website at DOI: 10.1021/acs.nanolett.8b03818.

Figures showing transfer curves, Au NP morphology, AFM images,a home-built PDMS microfluidic channel, response curves, the charge the device current, sensor response, specificity detection, electrical properties changes, and two decorated modes of target DNA; additional details on the reliability study and estimation of the number of target DNA molecules and carrier density change; and a table showing the response of five devices (PDF)

■ AUTHOR INFORMATION

Corresponding Authors

*E-mail: zyzhang@pku.edu.cn.

*E-mail: gyzhang@aphy.iphy.ac.cn.

ORCID

Guangyu Zhang: 0000-0002-1833-7598

Zhiyong Zhang: 0000-0003-1622-3447

Author Contributions

‖J.L., X.C., and Q.W. contributed equally to this work. Z.Z. proposed and supervised the project. Q.W and G.Z. synthesized the MoS_2 film by CVD and conducted material characterization by AFM. X.C designed DNA sequences and provided the initial DNA solution. J.L, M.X and W.S designed the device structure and test scheme. J.L. fabricated the sensor array and measured the sensors by electrical testing and Raman spectroscopy. J.L, Z.Z. and X.C analyzed the data and cowrote the manuscript. All authors discussed the results and commented on the manuscript.

Notes

The authors declare no competing financial interest.

■ ACKNOWLEDGMENTS

This work was supported by the National Key Research & Development Program (grant nos. 2016YFA0201901), the National Science Foundation of China (grant nos. 61621061 and 61427901), and the Beijing Municipal Science and Technology Commission (grant no. D171100006617002 1-2).

■ REFERENCES

(1) National Down Syndrome Society Home Page. https://www.ndss.org/ (accessed Jan 26, 2019).

(2) Asim, A.; Kumar, A.; Muthuswamy, S.; Jain, S.; Agarwal, S. Down syndrome: an insight of the disease. *J. Biomed. Sci.* **2015**, *22*, 41.

(3) Benn, P.; Borrell, A.; Chiu, R. W.; Cuckle, H.; Dugoff, L.; Faas, B.; Gross, S.; Huang, T.; Johnson, J.; Maymon, R.; et al. Position statement from the Chromosome Abnormality Screening Committee on behalf of the Board of the International Society for Prenatal Diagnosis. *Prenatal Diagn.* **2015**, *35*, 725−734.

(4) Salomon, L. J.; Alfirevic, Z.; Berghella, V.; Bilardo, C.; Hernandez-Andrade, E.; Johnsen, S. L.; Kalache, K.; Leung, K. Y.; Malinger, G.; Munoz, H.; et al. *Ultrasound Obstet Gynecol* **2011**, *37*, 116−126.

(5) Chiu, R. W.; Chan, K. A.; Gao, Y.; Lau, V. Y.; Zheng, W.; Leung, T. Y.; Foo, C. H.; Xie, B.; Tsui, N. B.; Lun, F. M.; et al. *Proc. Natl. Acad. Sci. U. S. A.* **2008**, *105*, 20458−20463.

(6) Taylor-Phillips, S.; Freeman, K.; Geppert, J.; Agbebiyi, A.; Uthman, O. A.; Madan, J.; Clarke, A.; Quenby, S.; Clarke, A. *BMJ. Open* **2016**, *6*, e010002.

(7) Lo, Y. D.; Tein, M. S.; Lau, T. K.; Haines, C. J.; Leung, T. N.; Poon, P. M.; Wainscoat, J. S.; Johnson, P. J.; Chang, A. M.; Hjelm, N. M. *Am. J. Hum. Genet.* **1998**, *62*, 768−775.

(8) Bunimovich, Y. L.; Shin, Y. S.; Yeo, W.-S.; Amori, M.; Kwong, G.; Heath, J. R. Quantitative real-time measurements of DNA hybridization with alkylated nonoxidized silicon nanowires in electrolyte solution. *J. Am. Chem. Soc.* **2006**, *128*, 16323−16331.

(9) Cai, B.; Wang, S.; Huang, L.; Ning, Y.; Zhang, Z.; Zhang, G.-J. Ultrasensitive label-free detection of PNA−DNA hybridization by reduced graphene oxide field-effect transistor biosensor. *ACS Nano* **2014**, *8*, 2632−2638.

(10) Cao, Y. C.; Jin, R.; Mirkin, C. A. Nanoparticles with Raman spectroscopic fingerprints for DNA and RNA detection. *Science* **2002**, *297*, 1536−1540.

(11) Stern, E.; Klemic, J. F.; Routenberg, D. A.; Wyrembak, P. N.; Turner-Evans, D. B.; Hamilton, A. D.; LaVan, D. A.; Fahmy, T. M.; Reed, M. A. Label-free immunodetection with CMOS-compatible semiconducting nanowires. *Nature* **2007**, *445*, 519.

(12) Nakatsuka, N.; Yang, K.-A.; Abendroth, J. M.; Cheung, K. M.; Xu, X.; Yang, H.; Zhao, C.; Zhu, B.; Rim, Y. S.; Yang, Y.; et al. *Science* **2018**, *362*, 319−324.

(13) Gao, A.; Lu, N.; Wang, Y.; Dai, P.; Li, T.; Gao, X.; Wang, Y.; Fan, C. Enhanced sensing of nucleic acids with silicon nanowire field effect transistor biosensors. *Nano Lett.* **2012**, *12*, 5262−5268.

DOI: 10.1021/acs.nanolett.8b03818
Nano Lett. XXXX, XXX, XXX−XXX

(14) Gao, Z.; Agarwal, A.; Trigg, A. D.; Singh, N.; Fang, C.; Tung, C.-H.; Fan, Y.; Buddharaju, K. D.; Kong, J. Silicon nanowire arrays for label-free detection of DNA. *Anal. Chem.* **2007**, *79*, 3291−3297.
(15) Hahm, J.-i.; Lieber, C. M. Direct ultrasensitive electrical detection of DNA and DNA sequence variations using nanowire nanosensors. *Nano Lett.* **2004**, *4*, 51−54.
(16) Hu, P.; Zhang, J.; Li, L.; Wang, Z.; O'Neill, W.; Estrela, P. Carbon nanostructure-based field-effect transistors for label-free chemical/biological sensors. *Sensors* **2010**, *10*, 5133−5159.
(17) Ko, J. W.; Woo, J.-M.; Jinhong, A.; Cheon, J. H.; Lim, J. H.; Kim, S. H.; Chun, H.; Kim, E.; Park, Y. J. Multi-order dynamic range DNA sensor using a gold decorated SWCNT random network. *ACS Nano* **2011**, *5* (6), 4365−4372.
(18) Xu, G.; Abbott, J.; Qin, L.; Yeung, K. Y.; Song, Y.; Yoon, H.; Kong, J.; Ham, D. Electrophoretic and field-effect graphene for all-electrical DNA array technology. *Nat. Commun.* **2014**, *5*, 4866.
(19) Maehashi, K.; Katsura, T.; Kerman, K.; Takamura, Y.; Matsumoto, K.; Tamiya, E. Label-free protein biosensor based on aptamer-modified carbon nanotube field-effect transistors. *Anal. Chem.* **2007**, *79* (2), 782−787.
(20) Martínez, M. T.; Tseng, Y.-C.; Ormategui, N.; Loinaz, I.; Eritja, R.; Bokor, J. Label-free DNA biosensors based on functionalized carbon nanotube field effect transistors. *Nano Lett.* **2009**, *9*, 530−536.
(21) Xu, S.; Zhan, J.; Man, B.; Jiang, S.; Yue, W.; Gao, S.; Guo, C.; Liu, H.; Li, Z.; Wang, J.; et al. Real-time reliable determination of binding kinetics of DNA hybridization using a multi-channel graphene biosensor. *Nat. Commun.* **2017**, *8*, 14902.
(22) Radisavljevic, B.; Radenovic, A.; Brivio, J.; Giacometti, i. V.; Kis, A. Single-layer MoS 2 transistors. *Nat. Nanotechnol.* **2011**, *6*, 147.
(23) Yin, Z.; Li, H.; Li, H.; Jiang, L.; Shi, Y.; Sun, Y.; Lu, G.; Zhang, Q.; Chen, X.; Zhang, H. Single-layer MoS_2 phototransistors. *ACS Nano* **2012**, *6*, 74−80.
(24) Lee, D.-W.; Lee, J.; Sohn, I. Y.; Kim, B.-Y.; Son, Y. M.; Bark, H.; Jung, J.; Choi, M.; Kim, T. H.; Lee, C.; et al. Field-effect transistor with a chemically synthesized MoS_2 sensing channel for label-free and highly sensitive electrical detection of DNA hybridization. *Nano Res.* **2015**, *8*, 2340−2350.
(25) Sarkar, D.; Liu, W.; Xie, X.; Anselmo, A. C.; Mitragotri, S.; Banerjee, K. MoS_2 field-effect transistor for next-generation label-free biosensors. *ACS Nano* **2014**, *8*, 3992−4003.
(26) Wang, L.; Wang, Y.; Wong, J. I.; Palacios, T.; Kong, J.; Yang, H. Y. Functionalized MoS_2 nanosheet-based field-effect biosensor for label-free sensitive detection of cancer marker proteins in solution. *Small* **2014**, *10* (6), 1101−1105.
(27) Yang, Y.; Ding, L.; Han, J.; Zhang, Z.; Peng, L.-M. High-performance complementary transistors and medium-scale integrated circuits based on carbon nanotube thin films. *ACS Nano* **2017**, *11*, 4124−4132.
(28) Zhong, D.; Zhang, Z.; Ding, L.; Han, J.; Xiao, M.; Si, J.; Xu, L.; Qiu, C.; Peng, L.-M. Gigahertz integrated circuits based on carbon nanotube films. *Nature Electronics* **2018**, *1*, 40.
(29) Huang, Z.; Chen, F.; Bennett, P. A.; Tao, N. Single molecule junctions formed via Au− thiol contact: stability and breakdown mechanism. *J. Am. Chem. Soc.* **2007**, *129*, 13225−13231.
(30) Shi, J.; Ma, D.; Han, G.-F.; Zhang, Y.; Ji, Q.; Gao, T.; Sun, J.; Song, X.; Li, C.; Zhang, Y.; et al. Controllable growth and transfer of monolayer MoS2 on Au foils and its potential application in hydrogen evolution reaction. *ACS Nano* **2014**, *8*, 10196−10204.
(31) Sreeprasad, T.; Nguyen, P.; Kim, N.; Berry, V. Controlled, defect-guided, metal-nanoparticle incorporation onto MoS_2 via chemical and microwave routes: electrical, thermal, and structural properties. *Nano Lett.* **2013**, *13*, 4434−4441.
(32) Zou, X.; Wang, J.; Chiu, C. H.; Wu, Y.; Xiao, X.; Jiang, C.; Wu, W. W.; Mai, L.; Chen, T.; Li, J.; et al. Interface Engineering for High-Performance Top-Gated MoS_2 Field-Effect Transistors. *Adv. Mater.* **2014**, *26*, 6255−6261.
(33) Rosenblatt, S.; Yaish, Y.; Park, J.; Gore, J.; Sazonova, V.; McEuen, P. L. High performance electrolyte gated carbon nanotube transistors. *Nano Lett.* **2002**, *2*, 869−872.
(34) Shimotani, H.; Kanbara, T.; Iwasa, Y.; Tsukagoshi, K.; Aoyagi, Y.; Kataura, H. Gate capacitance in electrochemical transistor of single-walled carbon nanotube. *Appl. Phys. Lett.* **2006**, *88*, 073104.
(35) Singha, S. S.; Nandi, D.; Singha, A. Tuning the photo-luminescence and ultrasensitive trace detection properties of few-layer MoS_2 by decoration with gold nanoparticles. *RSC Adv.* **2015**, *5*, 24188−24193.
(36) Chakraborty, B.; Bera, A.; Muthu, D.; Bhowmick, S.; Waghmare, U. V.; Sood, A. Symmetry-dependent phonon renormalization in monolayer MoS_2 transistor. *Phys. Rev. B: Condens. Matter Mater. Phys.* **2012**, *85*, 161403.
(37) Zhang, G.-J.; Chua, J. H.; Chee, R.-E.; Agarwal, A.; Wong, S. M.; Buddharaju, K. D.; Balasubramanian, N. Highly sensitive measurements of PNA-DNA hybridization using oxide-etched silicon nanowire biosensors. *Biosens. Bioelectron.* **2008**, *23*, 1701−1707.
(38) Li, Z.; Chen, Y.; Li, X.; Kamins, T.; Nauka, K.; Williams, R. S. Sequence-specific label-free DNA sensors based on silicon nanowires. *Nano Lett.* **2004**, *4*, 245−247.
(39) Stern, E.; Wagner, R.; Sigworth, F. J.; Breaker, R.; Fahmy, T. M.; Reed, M. A. Importance of the Debye screening length on nanowire field effect transistor sensors. *Nano Lett.* **2007**, *7*, 3405−3409.
(40) Zhang, G.-J.; Zhang, G.; Chua, J. H.; Chee, R.-E.; Wong, E. H.; Agarwal, A.; Buddharaju, K. D.; Singh, N.; Gao, Z.; Balasubramanian, N. DNA sensing by silicon nanowire: charge layer distance dependence. *Nano Lett.* **2008**, *8*, 1066−1070.
(41) Wilson, J. S. *Sensor Technology Handbook*; Elsevier: Amsterdam, The Netherlands, 2004, p 163.
(42) Kurkina, T.; Vlandas, A.; Ahmad, A.; Kern, K.; Balasubramanian, K. Label-free detection of few copies of DNA with carbon nanotube impedance biosensors. *Angew. Chem., Int. Ed.* **2011**, *50*, 3710−3714.
(43) Star, A.; Tu, E.; Niemann, J.; Gabriel, J.-C. P.; Joiner, C. S.; Valcke, C. Label-free detection of DNA hybridization using carbon nanotube network field-effect transistors. *Proc. Natl. Acad. Sci. U. S. A.* **2006**, *103*, 921−926.
(44) Gao, Z.; Xia, H.; Zauberman, J.; Tomaiuolo, M.; Ping, J.; Zhang, Q.; Ducos, P.; Ye, H.; Wang, S.; Yang, X.; et al. Detection of Sub-fM DNA with Target Recycling and Self-Assembly Amplification on Graphene Field Effect Biosensors. *Nano Lett.* **2018**, *18*, 3509−3515.
(45) Jin, K.; Xie, L.; Tian, Y.; Liu, D. Au-modified monolayer MoS_2 sensor for DNA detection. *J. Phys. Chem. C* **2016**, *120*, 11204−11209.
(46) Zhang, J.; Yu, H.; Chen, W.; Tian, X.; Liu, D.; Cheng, M.; Xie, G.; Yang, W.; Yang, R.; Bai, X.; et al. Scalable growth of high-quality polycrystalline MoS_2 monolayers on SiO_2 with tunable grain sizes. *ACS Nano* **2014**, *8*, 6024−6030.

DOI: 10.1021/acs.nanolett.8b03818
Nano Lett. XXXX, XXX, XXX−XXX